

## Total cross sections and analyzing powers for the reaction $p + p \rightarrow p + p + \pi^0$ near threshold

S. Stanislaus,\* D. Horváth,<sup>†</sup> D. F. Measday, and A. J. Noble

*Department of Physics, University of British Columbia, Vancouver, British Columbia, Canada V6T 1Z1*

M. Salomon

*TRIUMF, 4004 Wesbrook Mall, Vancouver, British Columbia, Canada V6T 2A3*

(Received 21 September 1990; revised manuscript received 3 June 1991)

We have studied the reaction  $p + p \rightarrow p + p + \pi^0$  from 320 to 500 MeV by detecting the  $\gamma$  rays from  $\pi^0$  decay in coincidence in two large NaI crystals. The obtained differential and total cross sections of the pions are in agreement with previous measurements but are of a higher precision. We have also measured the pion analyzing powers; the first measurement of this observable. Our results are compared with those for the reactions  $np \rightarrow NN\pi^\pm$  with confusing conclusions concerning the contribution of  $\sigma_{01}$ , the zero isospin pion production channel.

### I. INTRODUCTION

Pion production in nucleon-nucleon collisions has been much studied over the last 35 years. For pion production reactions near threshold, Watson and Brueckner [1] showed that the characteristics of the data could be conveniently analyzed in terms of angular momentum, parity, and isotopic spin conservation. In the notation of Rosenfeld [2], the total cross section for a reaction is denoted by  $\sigma_{if}$  where  $i$  is the initial and  $f$  is the final isotopic spin of the two-nucleon system. Thus for single pion production there are four cross sections,  $\sigma_{10}(d)$ ,  $\sigma_{10}(np)$ ,  $\sigma_{11}$ , and  $\sigma_{01}$ , where  $\sigma_{10}(d)$  and  $\sigma_{10}(np)$  represent the reactions with a deuteron and an unbound neutron and proton in the final state, respectively. All the possible reactions can be expressed in terms of these independent cross sections and are listed in Table I.

A very clean feature of the reaction

$$p + p \rightarrow p + p + \pi^0 \quad (1)$$

is that it involves only  $\sigma_{11}$ . Similarly,  $\sigma_{10}(d)$  can be independently measured and of the four elementary cross sections this has been the one most extensively studied. A full amplitude analysis of  $pp \rightarrow \pi^+ d$  has been attempted [3,4] and most major amplitudes are now fairly well determined. As for  $\sigma_{10}(np)$ , the cross section is reasonably well established at the present time; there are some asymmetry and spin-transfer data, as well, but by no means a complete set of measurements.

Using all the available experimental data from pion production reactions a phase-shift analysis has been done by VerWest and Arndt [5] who have thus determined the relative strengths of the four elementary cross sections. Bystricky *et al.* [6] used all the available data on inelastic nucleon-nucleon scattering and did a consistent fit and found that below 600 MeV  $\sigma_{01}$  was small although not negligible.

In fact, there has been a long and complex history as to whether  $\sigma_{01}$  is indeed nonzero. In Mandelstam's isobar model [7], for example, which ascribes the pion produc-

tion to excitation of a nucleon to a  $\Delta$  and to its subsequent decay to a nucleon and a pion,  $NN \rightarrow N\Delta \rightarrow NN\pi$ , the intermediate state can have an isospin of  $(\frac{1}{2} \pm \frac{1}{2})$ . Therefore, if isospin is conserved, there can be no pion production from an initial  $I=0$  state in the  $np$  reaction. Hence  $\sigma_{01}$  can occur only via other mechanisms and would be smaller than the main channels.

If  $\sigma_{01}$  was actually zero, the reactions  $np \rightarrow NN\pi^\pm$  would be identical to  $pp \rightarrow pp\pi^0$ , and so in the angular distribution of the pions, a  $\cos\theta$  term would be forbidden. Handler [8] in 1965 presented clear evidence for a fairly large  $\cos\theta$  term for the reaction  $np \rightarrow pp\pi^-$  at 409 MeV, while at SIN, Kleinschmidt *et al.* [9] hypothesized that  $\sigma_{01}$  was small for  $np \rightarrow nn\pi^+$  between 470 and 590 MeV. Unfortunately the latter measurement lacked sufficient angular information as they studied only small angles up to  $35^\circ$  in the center of mass. The recent results of the same group [10], combined with the earlier measurements, seem to indicate the existence of a fairly significant  $\cos\theta$  term very much in line with Handler and with some Dubna work at 600 MeV [11]. However, at 800 MeV the LAMPF experiment of Thomas *et al.* [12] studied both  $\pi^+$  and  $\pi^-$  producing  $np$  reactions quite extensively and found little evidence for a  $\cos\theta$  term or for  $\sigma_{01}$ . The total cross-section measurement by Dakhno *et al.* [13] from Gatchina also shows that  $\sigma_{01}$  is small. However, their bubble chamber experiment used protons onto deuterons so the interpretation is complicated by the presence of a spectator proton. Thus the situation is still fairly uncertain regarding the exact characteristics of  $\sigma_{01}$ .

The first cross section for the reaction  $pp \rightarrow pp\pi^0$  was measured at the University of Chicago by Marshall *et al.* [14] to be  $450 \pm 150 \mu\text{b}$  at an incident proton energy of 430 MeV. Since then a number of other near threshold investigations have been done by Mather and Martinelli [15], Soroko [16], Moyer and Squire [17], Prokoshkin and Tiapkin [18], Stallwood *et al.* [19], Dunaitsev and Prokoshkin [20], and Shimizu *et al.*, [21]. Except for the last, all of those were done during the period 1953 to 1959, the most extensive investigations being those of

TABLE I. Isotopic spin decomposition for total cross sections.

	Reaction	Isotopic spin decomposition
(a)	$p + p \rightarrow d + \pi^+$	$\sigma_{10}(d)$
(b)	$p + p \rightarrow n + p + \pi^+$	$\sigma_{10}(np) + \sigma_{11}$
(c)	$p + p \rightarrow p + p + \pi^0$	$\sigma_{11}$
(d)	$n + p \rightarrow d + \pi^0$	$\frac{1}{2}\sigma_{10}(d)$
(e)	$n + p \rightarrow n + p + \pi^0$	$\frac{1}{2}[\sigma_{10}(np) + \sigma_{01}]$
(f)	$n + p \rightarrow n + n + \pi^+$	$\frac{1}{2}[\sigma_{11} + \sigma_{01}]$
(g)	$n + p \rightarrow p + p + \pi^-$	$\frac{1}{2}[\sigma_{11} + \sigma_{01}]$

Stallwood *et al.* and Dunaitsev and Prokoshkin. Most of these measurements are effectively total cross sections and near threshold the quality is fairly poor. The bubble chamber experiment done at KEK by Shimizu *et al.* [21] produced a large set of useful data on pion production in the  $pp$  system for  $325 < T_p < 1262$  MeV, however, their two points below 500 MeV on the reaction  $pp \rightarrow pp\pi^0$  are clearly higher than all other data (including ours). Recently, at the Indiana University Cooler, Meyer *et al.* [22] have made a very clean measurement of the cross sections very near to the threshold (282–325 MeV), extracting some very useful information on the  $s$ -wave pion production.

Except for the measurements of Dunaitsev and Prokoshkin [20], all other experiments in our energy region have determined only the total cross sections of reaction (1). Dunaitsev and Prokoshkin were able to obtain the angular distribution of the pions from the  $\gamma$ -ray spectra, but the quality of their results is not very good, mainly because of the very poor information they had on the energy distribution of the  $\gamma$  rays. The only experiment that had fairly good energy information was that of Cence *et al.* [23], but this was done at the higher energy of 735 MeV. From their  $\gamma$ -ray energy spectra they were able to deduce the  $\pi^0$  energy spectra in the center-of-mass system.

The differential cross section for pion emission in the reaction  $pp \rightarrow pp\pi^0$  is normally described by

$$\left( \frac{d\sigma}{d\Omega} \right) \propto \frac{1}{3} + b \cos^2\theta, \quad (2)$$

where  $\theta$  is the  $\pi^0$  angle in c.m. system and  $b$  is the angular distribution parameter. (Odd powers of  $\cos\theta$  are forbidden.) Dunaitsev and Prokoshkin [20] found  $b = 0.06 \pm 0.06$  between 400 and 675 MeV, Guzhavin *et al.* observed  $0.04 \pm 0.015$  at 650 MeV [24], whereas at 735 MeV Cence *et al.* [23] obtained  $b = 0.27 \pm 0.04$ .

The situation with regard to the theory is somewhat rudimentary as none of the numerous existing models can provide a consistent picture of the existing  $NN \rightarrow NN\pi$  data. The Mandelstam [7] model described the gross features and has been retained in most subsequent calculations. In the 1960s most of the calculations were centered on the soft pion approach [25–28] of peripheral calculations [29,30]. Recently there have been a number of

new calculations [31–36,38–40], the most successful being the Faddeev approach of Dubach, Kloet, and Silbar [40]. A new endeavor has been to incorporate quark effects into the calculations [41,42]. However, none of the models has been very successful in reproducing the overall experimental results, and are, at best, only in qualitative agreement with some experimental data. For most existing models, no predictions have been made for the reaction  $pp \rightarrow pp\pi^0$  mainly because there are not enough data with which to compare the calculations. Because the reaction  $pp \rightarrow pp\pi^0$  has been studied to some extent, it can be used as a guide when other production reactions are being debated. Thus it was used as a calibration by Choi, Kang, and Kim [43] when they estimated axion production via nucleon-nucleon axion bremsstrahlung.

## II. THE EXPERIMENT

The experiment was carried out using the polarized protons of the primary beam line (1B) at TRIUMF. The main features of the experimental setup are depicted in Fig. 1. A liquid-hydrogen target was bombarded by polarized protons and the two  $\gamma$  rays from the  $\pi^0$  decay were detected in coincidence. Our  $\pi^0$  spectrometer [44] consisted of two large NaI(Tl) crystals, TINA (46 cm o.d.  $\times$  51 cm) and MINA (36 cm o.d.  $\times$  36 cm), with a plastic scintillator in front of each crystal for the rejection of charged particles. Each NaI crystal was viewed by seven phototubes. In order to improve the energy resolution of the NaI crystals, and to protect them from

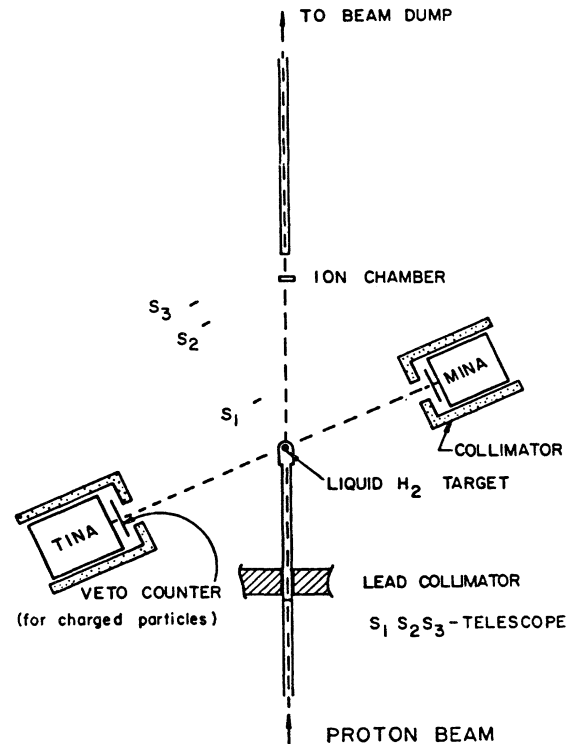


FIG. 1. Schematic of the experimental setup.

scattered protons, TINA and MINA were equipped with 20 cm thick, 30 and 25 cm i.d. iron collimators. The crystals were kept at a large distance of 125 cm from the target, at the expense of solid angle, in order to be able to distinguish the  $\pi^0$  photons from the copious background neutrons, using the time-of-flight method. The time of flight of the neutral particles was measured relative to the 43 ns rf signal of the cyclotron as the beam intensity was too high to use beam monitor counters.

The liquid-hydrogen target was a vertical cylinder, with the dimensions 5 cm i.d.  $\times$  5 cm selected to minimize the energy loss of the incident protons in the target while still giving a reasonable event rate. The walls of the  $H_2$  flask were made of 0.13-mm-thick Kapton. The flask was contained in an evacuated scattering chamber with a large window also made of 0.13-mm-thick Kapton.

The two arms of the  $\pi^0$  spectrometer were timed together using the protons scattered at  $41.5^\circ$  from the  $pp \rightarrow pp$  elastic scattering at 497 MeV incident energy. The  $\pi^0$  events were triggered by a coincidence between neutral particles in TINA and MINA. An event recorded the following information: (i) Pulse heights of individual tubes of the spectrometer as well as the total energies deposited in TINA and MINA. (ii) Time of flight of the neutral particles to TINA and MINA. (iii) The spin direction of the incident beam.

The experiment was run at proton energies of 320, 350, 403, 450, and 497 MeV. The beam energies were known to 1 MeV. Various combinations of angles were used: several measurements with TINA and MINA at  $180^\circ$  to each other ( $40^\circ$ - $140^\circ$ ,  $60^\circ$ - $120^\circ$ ,  $80^\circ$ - $100^\circ$ ) and others at symmetric angles ( $40^\circ$ - $40^\circ$ ,  $60^\circ$ - $60^\circ$ ,  $70^\circ$ - $70^\circ$ ,  $80^\circ$ - $80^\circ$ ,  $90^\circ$ - $90^\circ$ ), where the two angles refer to the laboratory angles of TINA and MINA, respectively. In all  $180^\circ$  geometries TINA was always kept at backward angles, mainly to protect it from large fluxes of particles, it being the better and the larger of the crystals. Data were accumulated in short runs and at the end of each full target run, an empty-target run was performed to measure the  $\pi^0$  background produced from the walls of the target flask.

The beam current was monitored using a polarimeter upstream, an ion chamber downstream, as well as a telescope at  $30^\circ$  consisting of three plastic scintillators which detected all scattered charged particles (but mainly elastically scattered protons). Of these the polarimeter was the primary beam monitor, the others were used for consistency checks only. In order to be able to measure the beam current, the polarimeter was calibrated by stopping the beam in a Faraday cup.

The beam current that could be used was limited by the pile up in MINA (or in both TINA and MINA at symmetric geometries). Typically, the current was varied from about 20 pA at 500 MeV for a  $40^\circ$ - $140^\circ$  geometry to about 250 pA at 320 MeV for a  $90^\circ$ - $90^\circ$  geometry. The polarization was typically 40–70%, depending on the condition of the ion source.

### III. DATA ANALYSIS

The neutral particles detected by TINA and MINA consisted of neutrons and  $\gamma$  rays, thus the hardware

trigger selected  $\gamma$ - $\gamma$ ,  $n$ - $\gamma$ , and  $n$ - $n$  events. Most of the neutron-related background events were removed from the data set by imposing a cut on the time of flight (TOF) of the detected particles. Figure 2 shows typical TOF spectra. The photons have a TOF of  $\sim 4.1$  ns from the target to the detectors, whereas the TOF of the neutrons is a function of their kinetic energy. The double spectrum shown in Fig. 2 was a result of vetoing every other rf pulse. This ensured that we saw the entire rf spectrum and also gave us a way of calibrating the TDCs.

Figure 2(a) corresponds to the  $180^\circ$  geometry with both TINA and MINA at  $90^\circ$ , and in Fig. 2(b) both detectors were at forward angles. Since most of the background neutrons tend to travel forward in the laboratory, it can be clearly seen that the rate of neutron related events increased as the arms of the spectrometer were moved to forward angles. A “cut” was imposed on the rf spectra to reject the neutron events by setting windows on the time of flight of the detected particles. The cuts were determined by fitting to the spectra a function which consisted of a Gaussian term for the  $\gamma$  peaks and an asymmetric function for the neutron peaks.

There were two types of TOF cuts in the analysis, one to extract the total and differential cross sections and another for the analyzing powers. For the cross section it was essential that no  $\pi^0$  events be lost, so a window of  $\pm 3\sigma$  (where  $\sigma$  is the standard deviation) on the  $\gamma$  peaks was selected for all  $\gamma$  events. The efficiency of the TOF cut was always above 95% of the signal. Suitable correc-

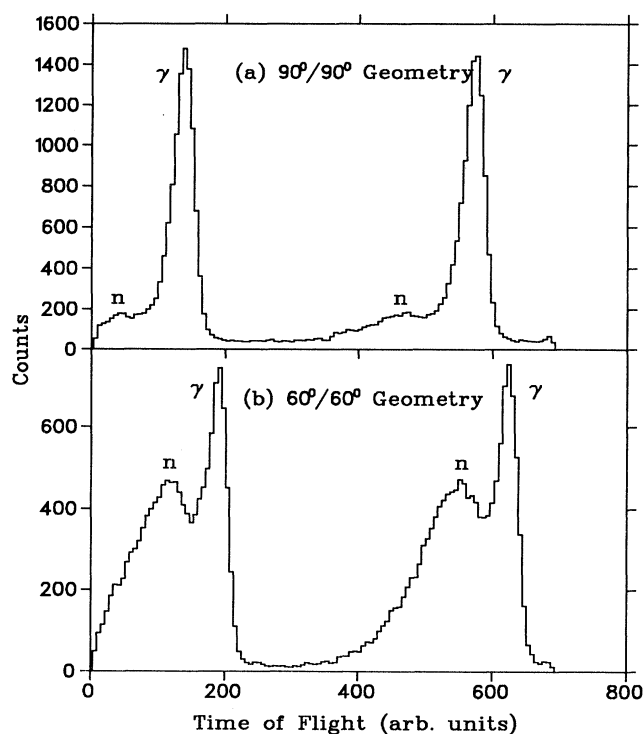


FIG. 2. Time of flight of neutral particles to TINA for (a)  $180^\circ$  geometry and (b) forward symmetric geometry.

tions were made to account for the inefficiencies caused by the time walk of the rf signal. As seen in Fig. 2, the tail of the neutron peak overlaps with the  $\gamma$  peak. Since these neutrons could influence the results, a narrower window ( $\pm 2\sigma$ ) was placed on the  $\gamma$  peaks when determining the analyzing powers.

When a  $\pi^0$  decays into two photons of energy  $E_1$  and  $E_2$ , it can be shown that

$$E_1 E_2 = \frac{m_{\pi^0}^2}{4 \sin^2(\psi/2)}, \quad (3)$$

where  $\psi$  is the opening angle between the two  $\gamma$  rays. This is very important as it means that  $E_1 E_2$  is independent of the  $\pi^0$  energy. For a given geometry of the  $\pi^0$  spectrometer (i.e., at  $\psi = \text{const}$ ) this represents a hyperbola. With most of the neutrons removed using the TOF cut, a two-dimensional plot of energy deposited in MINA against energy deposited in TINA (Fig. 3) shows this hyperbolic band very clearly. The  $\pi^0$  mesons show up as a peak in a spectrum of  $E_T E_M$  [Fig. 4(a)]. The background seen in Fig. 3 and the low-energy tail of Fig. 4(a) correspond to the background events underneath the  $\gamma$  peaks of Fig. 2.

The efficiency of the TOF cut was checked by looking at the events discarded by the TOF cut [Fig. 4(b)]. In a few runs a small peak showed up in the position of the  $\pi^0$  mass, as a result of a time walk of the rf signal. For these runs the TOF cut for the cross-section analysis was slightly loosened until this secondary peak was below the 5% level. A window was set on the mass spectra to separate the  $\pi^0$  events from the background events. This effectively removed all the background events. The position of the window was determined by fitting an asymmetric peak to the mass spectra. The background underneath the  $\pi^0$  mass peak was estimated to be less than 2%.

In the analysis of the cross-section data, the number of pions lost due to the TOF cut was estimated by fitting the

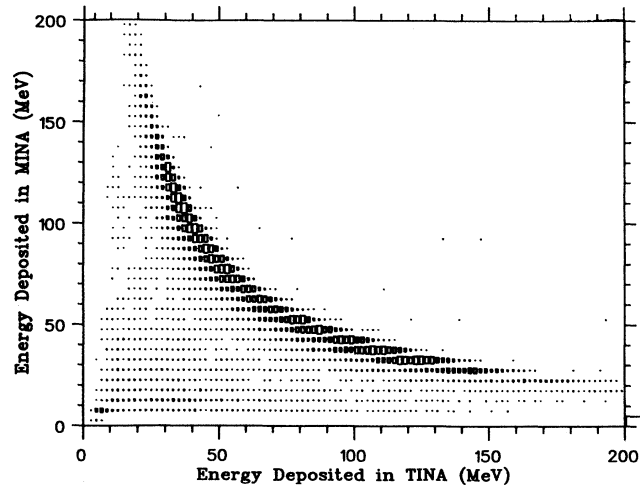


FIG. 3. Two-dimensional plot of energy deposited in MINA against energy deposited in TINA. The hyperbolic band corresponds to  $\pi^0$  production.

same asymmetric function to the background mass spectra [Fig. 4(b)]. These losses were later used to renormalize the  $\pi^0$  energy spectra.

The two cuts mentioned above helped to remove the background related to the  $n-\gamma$ ,  $n-n$  events and random coincidences. That left behind the much larger background of neutral pions from substances other than the liquid hydrogen in the target. At each geometry of the spectrometer several runs were recorded with the target full and the target empty. Here the target full refers to the target flask filled with liquid hydrogen. In the analysis, after applying the first two cuts, normalised empty-target runs were subtracted from the corresponding full target runs. This ensured the removal of this  $\pi^0$  background, and produced the final spectra to be used later for deducing the cross sections and analyzing powers.

The NaI energy spectra were calibrated using the maximum photon energy produced by the decay of the  $\pi^0$  from  $pp \rightarrow pp\pi^0$ , at each position of TINA and MINA. Only the  $180^\circ$  geometry was used for the calibration where the direction of the  $\pi^0$  is fairly precisely defined. The cutoff energies were determined by fitting a function to the high-energy part of the  $\gamma$  spectra.

In addition to the above, information from  $pp$  elastic scattering could also be used for calibration. At low energies ( $< 20$  MeV) the light produced in NaI from a proton is slightly less than that from an electron or  $\gamma$  ray of equivalent energy but at higher energies the difference is minimal. A comparison of  $\gamma$ -ray and proton calibration is illustrated in Fig. 5. The slight gain shifts in the photo-

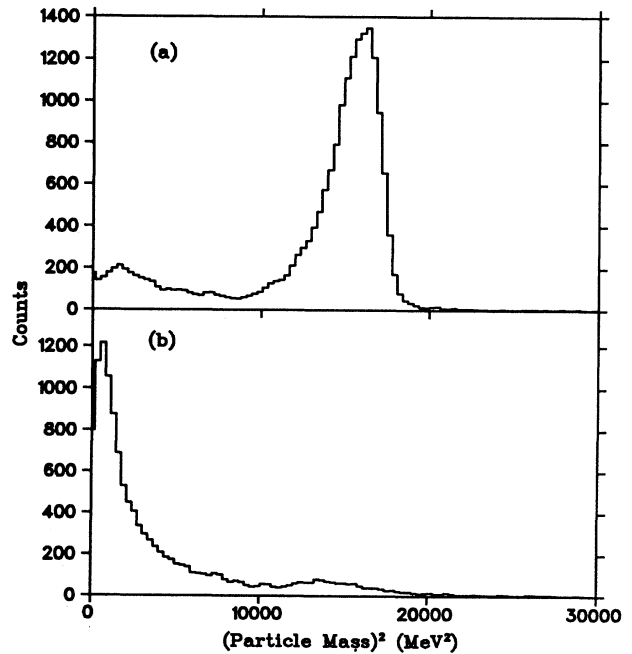


FIG. 4. The spectrum of  $ETINA \cdot EMINA$  (a) for events inside the TOF window. The peak corresponds to  $\pi^0$  production; (b) for events outside the TOF window.

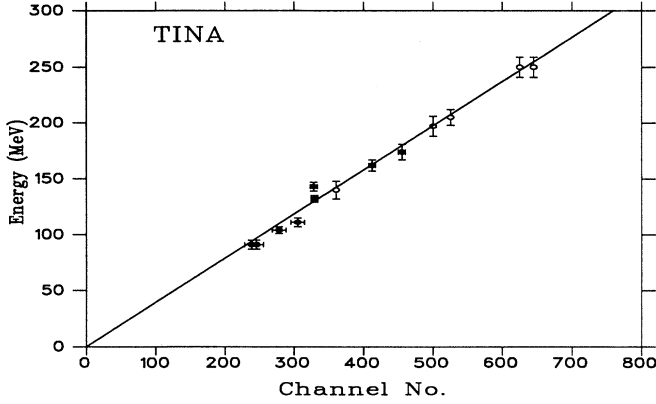


FIG. 5. Energy calibration of TINA. The closed circles are from  $\gamma$  spectra and the open circles are from proton scattering.

tubes due to different fluxes of charged particles were accounted for in the analysis.

The response of TINA and MINA to a monoenergetic  $\gamma$  ray can be fairly well described by the empirical function [45]

$$P(E_\gamma, A, B, C, D) = A \exp\left[\frac{E_\gamma - B}{D}\right] \left[1 - \operatorname{erf}\left[\frac{E_\gamma - B}{C}\right]\right], \quad (4)$$

where  $A$  is the amplitude,  $B$  is the peak position, and  $C$  and  $D$  are the half widths related to the high- and low-energy tails of the peak, respectively. The energy dependence of the parameters  $C$  and  $D$  was determined from Monte Carlo simulations using the *EGS* code [46] and was obtained as

$$C = C_0 E_\gamma^{0.8} \quad \text{and} \quad D = D_0 E_\gamma^{0.6}, \quad (5)$$

where  $C_0$  and  $D_0$  are parameters related to the resolution of the detector. This is in agreement with other experimental observations [47].

The spectrometer measured the energy of the  $\pi^0$  as the sum of the energies deposited in TINA and MINA. The overall detection efficiency of the spectrometer was determined using the Monte Carlo method assuming that the pions created in the reaction  $pp \rightarrow pp\pi^0$  have an isotropic angular distribution in the center of mass. In the energy region of this experiment this is nearly so (see Ref. [20] and later). The results of the Monte Carlo program were checked against the analytical calculations using the method of intersecting cones [44] for a point target, and the agreement was very good. Figure 6 shows the  $\pi^0$  detection efficiency as a function of the  $\pi^0$  kinetic energy.

#### A. Total and differential cross sections

The energy of the  $\pi^0$  was defined as the sum of the energies deposited in TINA and MINA and then the  $\pi^0$  energy spectra were used to determine the cross sections. Since only the  $180^\circ$  geometry data were used in this particular analysis, the direction of the  $\pi^0$  was either towards TINA or towards MINA, whichever had the higher ener-

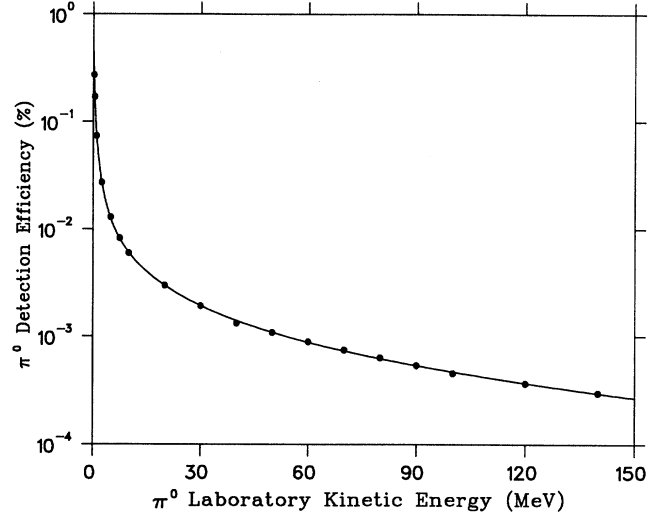


FIG. 6. The  $\pi^0$  detection efficiency (geometrical) as a function of the  $\pi^0$  kinetic energy. The data points are results from Monte Carlo simulation and the solid line is a fit to the data.

gy deposited. Table II lists the information on the  $\pi^0$  energy spectra.

For the reaction  $pp \rightarrow pp\pi^0$ , the energy distribution of the  $\pi^0$  depends on the final states of the scattered protons and the  $\pi^0$ . The relative angular momenta of the nucleons and the pion serve as a convenient classification. Three categories are of interest in the energy region of the experiment. The  $\pi^0$  energy distributions in the center of mass have been derived by Gell Mann and Watson [48], under certain assumptions which are truly valid only near threshold. These energy distribution functions are

$$\left[\frac{d\sigma_{11}}{dT}\right]_{Ss} \propto \eta \frac{(T_0 - T)^{1/2}}{T_0 - T - B'}, \quad (6)$$

$$\left[\frac{d\sigma_{11}}{dT}\right]_{Ps} \propto \eta (T_0 - T)^{3/2}, \quad (7)$$

$$\left[\frac{d\sigma_{11}}{dT}\right]_{Pp} \propto \eta^3 (T_0 - T)^{3/2}, \quad (8)$$

where  $\eta$  is the  $\pi^0$  momentum,  $T_0$  is the maximum  $\pi^0$  kinetic energy, and  $B'$  is the energy of the two nucleons in a virtual  $^1S_0$  state ( $B' \simeq 60$  keV). The  $(S, P)$  indices refer to the relative angular momentum of the two nucleons in the final state while  $(s, p)$  refers to the angular momentum of the pion with respect to the center of mass of the two nucleons. Although there is an additional contribution due to the interference between  $Ps$  and  $Pp$  classes, it was not considered in the fit as that term will be approximately canceled out when integrated over all angles. Furthermore, these functional forms for the  $\pi^0$  energy distribution may not be perfect because of the assumptions made by Gell-Mann and Watson [48]. However, the fits that we obtained are quite satisfactory within our errors.

The  $Ss$  and  $Ps$  class distributions are isotropic in the center of mass whereas the  $Pp$  class has an additional

$\cos^2\theta$  term in the angular distribution (see Table III). The differential and total cross sections as well as the angular distribution parameter were determined by fitting to the experimental spectra the "theoretical" laboratory energy distributions from (6) through (8) created using the Monte Carlo method.

For each distribution  $\pi^0$  mesons were randomly generated isotropically in the center of mass, for the  $Pp$  class a  $\cos^2\theta$  angular distribution was also added. The energy and the direction of the pions were transformed from the center-of-mass frame to the laboratory frame and the energy spectra at the experimental laboratory angles were determined. These laboratory spectra were then corrected for the detection efficiency and the response of the spectrometer.

These calculated energy spectra along with background terms were then fitted to the experimental energy spectra, using the fitting routine MINUIT [49]. Since each laboratory angle covers a unique area of a  $\theta_{c.m.}$  vs  $E_{c.m.}$  space, in order to get an overall picture of the center of mass and to obtain the angular distribution of the differential cross section, it was essential to fit all the spectra for a given proton energy simultaneously. Furthermore, an added advantage in fitting all angles simul-

taneously is that the interference terms will approximately average out. Typical fits to the data are shown in Fig. 7. The  $\chi^2$  per degree of freedom for the fits ranged from 0.88 to 1.05. The differential cross section can be expressed in the form

$$\left( \frac{d\sigma}{d\Omega} \right)_{c.m.} = \frac{K \times 0.8 \times 10^{-6}}{4\pi} \times \left[ \sum_{i=1}^3 A_i + A_4 \cos^2\theta \right] \text{ mb/sr}, \quad (9)$$

where  $K$  is the calibration factor of the polarimeter and  $A_i$  are the cross sections associated with the  $Ss$ ,  $Ps$ , and isotropic part of  $Pp$ , respectively, and  $A_4$  is associated with the anisotropic part of  $Pp$ . Since the two protons are indistinguishable in the center-of-mass frame, in a Legendre-polynomial expansion of the angular distribution only even powers of  $\cos\theta$  can appear. Also, there is experimental evidence [23] that powers of four and above are not required to describe the angular distribution in the energy region of this experiment and hence

TABLE II. Statistics of  $\pi^0$  spectra.

Proton energy (MeV)	Lab angle (deg)	Number of $\pi^0$ events	Total number of $\pi^0$ events
496	40	5013	47375
	60	4758	
	80	3495	
	90	23114	
	100	3364	
	120	3535	
	140	4096	
450	40	6413	64387
	60	8010	
	80	9445	
	90	22334	
	100	8417	
	120	5820	
	140	3948	
402	40	6349	44865
	60	7874	
	80	6018	
	90	11910	
	100	5600	
	120	4513	
	140	2601	
349	60	3195	17413
	80	5445	
	90	8252	
	100	3716	
	129	797	
319	90	10139	10139

TABLE III. Transitions of low partial waves which describe  $\sigma_{11}$ , the single pion production reaction  $p + p \rightarrow p + p + \pi^0$ .

Class	Initial state	Final state	Pion angular distribution	Energy dependence
$Ss$	${}^3P_0$	${}^1S_0s_0$	Isotropic	$\eta_0^2$
$Ps$	${}^1S_0$	${}^3P_0s_0$	Isotropic	$\eta_0^6$
	${}^1D_2$	${}^3P_2s_2$	Isotropic	$\eta_0^6$
$Pp$	${}^3P_1$	${}^3P_0p_1$	$C + \cos^2\theta$	$\eta_0^8$
	${}^3P_{0,1,2}$ or ${}^3F_2$	${}^3P_{1p_{0,1,2}}$	$C + \cos^2\theta$	$\eta_0^8$
	${}^3P_{1,2}$ or ${}^3F_{2,3}$	${}^3P_{2p_{1,2,3}}$	$C + \cos^2\theta$	$\eta_0^8$

$$\left( \frac{d\sigma}{d\Omega} \right)_{\text{c.m.}} = a_0 + 6a_2 \left( \cos^2\theta - \frac{1}{3} \right). \quad (10)$$

$$b = \frac{A_4}{3 \sum_{i=1}^3 A_i}. \quad (13)$$

The total cross section is given by

$$\sigma_T = 4\pi a_0 = 0.8 \times 10^{-6} K \left[ \sum_{i=1}^3 A_i + \frac{A_4}{3} \right] \text{ mb}. \quad (11)$$

It is normal practice [20] to express the differential cross section as

$$\left( \frac{d\sigma}{d\Omega} \right)_{\text{c.m.}} \propto \frac{1}{3} + b \cos^2\theta. \quad (12)$$

From Eqs. (10) and (12) the angular distribution parameter  $b$  can be obtained as

Since the polarimeter calibration had an uncertainty of about 4%, its effect on the results was checked by redoing the above fits, varying the number of incident protons randomly up to 4%. The resulting values of the parameters were within the errors of the original parameters.

In order to check the sensitivity of the results to the resolution of the spectrometer, the resolution was changed arbitrarily and the data were reanalysed. Use of a 20% better resolution produced a total cross section of about 4% less than the values obtained earlier. Hence a small uncertainty in the resolution of the spectrometer will not affect the final result.

Instead of fitting the experimental spectra with the center-of-mass energy distributions of  $Ss$ ,  $Ps$ , and  $Pp$  classes given by Gell-Mann, an attempt was made to fit the experimental data with a general function as well. Using the results obtained by Cence *et al.* [23] at 735 MeV as a guide, the center-of-mass energy distributions were defined by

$$f(T) = \alpha_1 T^{B_1} (T_0 - T)^{C_1} + \alpha_2 T^{B_2} (T_0 - T)^{C_2}, \quad (14)$$

where  $T_0$  is the maximum kinetic energy of the  $\pi^0$  in the center of mass,  $B_i$ ,  $C_i$  are parameters that define the shape of the center-of-mass spectrum, and  $\alpha_i$  are normalization parameters. Function (14) has two terms, both of which go naturally to zero at lower and higher energies. The lower-energy part of the  $\pi^0$  spectrum is described mainly by the first term and the higher-energy part mainly by the second term. Although fitting a general function of this form is difficult to perform, as every change in the powers involved a new Monte Carlo simulation, function (14) fitted the experimental spectra quite well and gave total cross sections identical to the ones obtained from the fits discussed earlier. A phase-space term was also allowed for in the fit, but was rejected during the iteration.

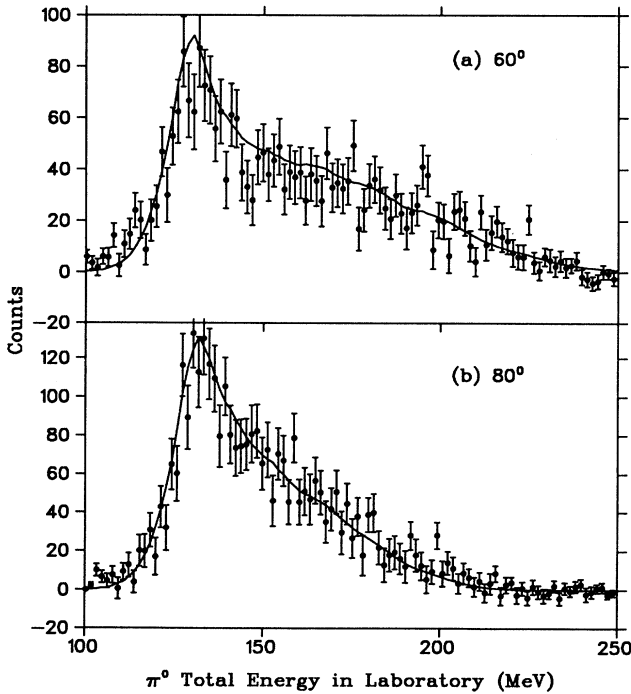


FIG. 7. The observed  $\pi^0$  energy spectra at (a)  $60^\circ$  and (b)  $80^\circ$  laboratory angles for 496 MeV incident proton energy. The spectra are not corrected for the efficiency of the detector. The solid line is a fit to the data.

## B. Analyzing power

As mentioned earlier, in order to ensure that the neutrons did not affect the analyzing powers of the  $\pi^0$  emission a narrower,  $\pm 2\sigma$  cut was imposed on the time of flight of the neutral particles when selecting the photon

events in TINA and MINA. When producing the final spectra to estimate the analyzing powers, the other cuts and background subtractions were done in the same way as for the cross-section data.

In the experiment two types of geometries were used, one with TINA and MINA at  $180^\circ$  to each other and the other at symmetric angles. The  $180^\circ$  geometry has the advantage that the direction of the  $\pi^0$  can be clearly defined. Except at very low  $\pi^0$  energies, the pions detected are those that move towards either TINA or MINA. The symmetrical geometry has the advantage that the left-right asymmetry can be observed in a clear and simple way because the higher-energy photon defines the left or right side for the  $\pi^0$  yet both sides are detected simultaneously. A major disadvantage of the symmetric geometry is that at these geometries the laboratory angle of the detected  $\pi^0$  is a function of its kinetic energy and had to be calculated from kinematics. In Fig. 8 is shown a two-dimensional Monte Carlo simulated energy spectrum of the  $\pi^0$  from the reaction  $pp \rightarrow pp\pi^0$  assuming an isotropic  $\pi^0$  angular distribution in the center of mass. The solid lines show the  $\pi^0$  laboratory angle as a function of the  $\pi^0$  laboratory kinetic energy for the geometries used in this experiment. This plot was used to define the angle of the  $\pi^0$  for symmetric geometries.

The  $\pi^0$  energy spectra were produced separately for the spin-up and spin-down states for both TINA and MINA in order to calculate the analyzing powers. The analyzing power is defined as the ratio of the polarized to unpolarized differential cross sections, i.e.,

$$A_N(\theta, T_\pi) = \frac{d\sigma_1}{d\Omega} / \frac{d\sigma_0}{d\Omega}. \quad (15)$$

This simplifies to [50]

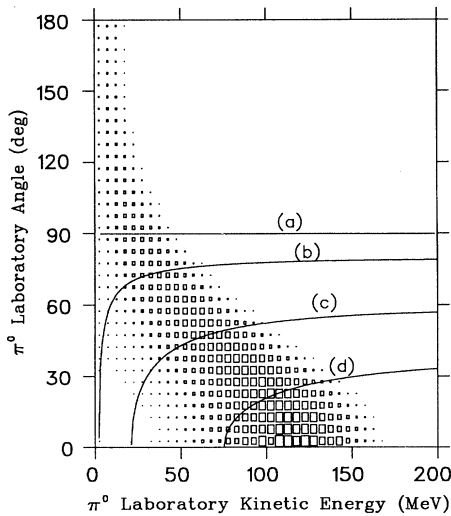


FIG. 8. Kinematics of the symmetric geometry at 450 MeV. The lines show the relationship between the direction and the energy of the  $\pi^0$  mesons detected at (a)  $90^\circ$ - $90^\circ$ , (b)  $80^\circ$ - $80^\circ$ , (c)  $60^\circ$ - $60^\circ$ , and (d)  $40^\circ$ - $40^\circ$ . The density plot is a Monte Carlo simulation of the  $\pi^0$  angular and energy distributions.

$$A_N(\theta, T_\pi) = \frac{N_{\pi^0}^+ / N_{LR}^+ - N_{\pi^0}^- / N_{LR}^-}{P^- N_{\pi^0}^+ / N_{LR}^+ + P^+ N_{\pi^0}^- / N_{LR}^-}, \quad (16)$$

where (i)  $N_{LR}^{+(-)}$  refer to the number of polarimeter counts at spin up (down), (ii)  $P^{+(-)}$  is the beam polarizations for spin-up (-down) state according to the Madison convention [51], and (iii)  $N_{\pi^0}^{+(-)}$  is the number of  $\pi^0$ 's detected at spin up (down). The sign of the analyzing power is positive if spin up preferentially produces  $\pi^0$ 's to the left.

For the symmetric geometry, since both TINA and MINA were at the same angle, the analyzing powers were determined separately and averaged.

## IV. RESULTS AND DISCUSSION

### A. Total cross sections

The results of our total cross-section measurements for the reaction  $pp \rightarrow pp\pi^0$  are given in Table IV and presented in Fig. 9 along with those of Dunaitsev and Prokoshkin [20], Stallwood *et al.* [19], Cence *et al.* [23], Shimizu *et al.* [21], and Marshall *et al.* [14] (we have not included the preliminary results of Reposeur *et al.* [52] as well as the recent near threshold results of Meyer *et al.* [22]). The errors quoted are those due to statistics and the uncertainty in the calibration of the polarimeter. As seen in the figure our results are in very good agreement with the previous measurements. The results of Dunaitsev and Prokoshkin are slightly higher than ours at lower energies while our results tend to be a bit higher at higher energies. The data set of Stallwood *et al.* are closer to our results, but the recent measurements of Shimizu *et al.* are systematically larger than all the others in our energy region. Our results are of much higher accuracy compared to the earlier measurements at higher energies ( $\geq 400$  MeV), while at lower energies (319 and 350 MeV) our error bars are slightly larger due to poor statistics and insufficient information on the  $\pi^0$  angular distribution. Near pion production threshold the cross sections are low, the background from  $\pi^0$  production on carbon is large and the data taking is limited by pile up due to elastic protons.

In the analysis, although fits were performed using the functional forms of the energy distributions derived by Gell-Mann and Watson [48], our total cross-section results are not model dependent because alternate fits with general functions produced identical results. The center-of-mass  $\pi^0$  energy spectra are illustrated in Fig. 10.

TABLE IV. Values of total cross section and the angular distribution parameter.

Proton energy (MeV)	$\sigma_T$ ( $\mu\text{b}$ )	$b_{\pi^0}$
496	$656 \pm 34$	$0.036 \pm 0.013$
450	$285 \pm 13$	$0.048 \pm 0.013$
402	$69 \pm 4$	$0.054 \pm 0.015$
349	$18.1 \pm 5.0$	$0.018 \pm 0.016$
319	$7.8 \pm_{3.0}^3.0$	$0.003 \pm 0.055$

The main differences between the present experiment and the previous ones are the following. (1) The energies of the decay  $\gamma$  rays were fairly precisely measured, whereas in previous measurements in this energy range the energy was not measured at all. Only Cence *et al.* [23] measured the  $\gamma$ -ray energy, but that was at a higher energy of 735 MeV. (2) Both decay  $\gamma$  rays were detected whereby the direction and the energy of the  $\pi^0$  mesons could be precisely determined. In previous experiments both the energy and the direction of the  $\pi^0$  were not directly measured but were obtained by fairly complicated fitting procedures.

### B. Angular distribution of the $\pi^0$

The results obtained for the  $b$  parameter in the  $\pi^0$  angular distribution are also listed in Table IV. The errors quoted are due to statistics and to the choice of the fitting function. Figure 11 presents our measurements of the  $\pi^0$  angular distribution parameter  $b$  along with the results of Dunaitsev and Prokoshkin [20], Cence *et al.* [23], and Guzhavin *et al.* [24]. The two solid lines represent the values of the parameter obtained from two global fits to the data [50,53], and the dotted lines are extrapolations to higher energies.

As seen in the figure, our results are consistent with the earlier measurements but of much higher precision. Dunaitsev and Prokoshkin obtained the angular distribution of the  $\pi^0$  mesons from measurements of the angular distribution of the  $\gamma$  rays from the decay of the  $\pi^0$ . The angular distributions of the  $\gamma$  rays and the  $\pi^0$  mesons are connected by relations, the analysis of which has shown

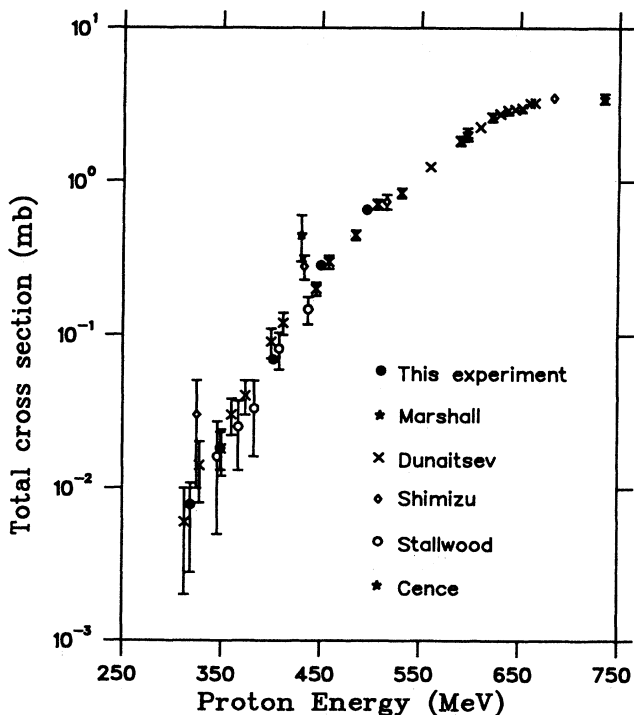


FIG. 9. Total cross sections for the reaction  $p + p \rightarrow p + p + \pi^0$ .

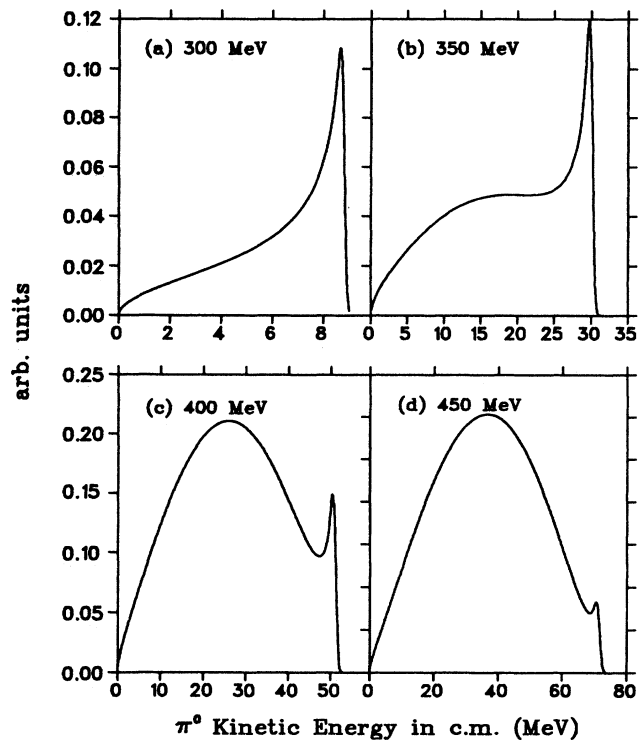


FIG. 10. The center-of-mass energy spectra of  $\pi^0$  at (a) 300 MeV, (b) 350 MeV, (c) 400 MeV, and (d) 450 MeV, calculated from the global fit parameters.

that even at higher energies and with an anisotropic distribution of the  $\pi^0$  mesons, the  $\gamma$ -ray angular distribution differs comparatively little from isotropic [18]. Only at  $\pi^0$  kinetic energies above 200 MeV does the angular distribution of the  $\gamma$ -rays approach that of the  $\pi^0$  mesons. This uncertainty is clearly demonstrated by the large error bars seen in their results. An accurate measurement

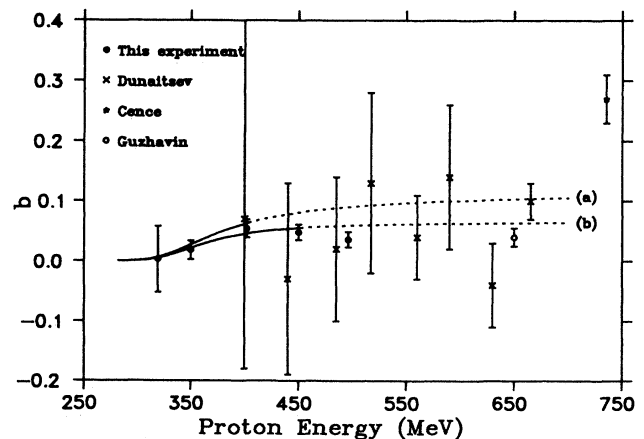


FIG. 11. Energy dependence of the  $\pi^0$  angular distribution parameter  $b$  from the relation  $d\sigma/d\Omega \propto \frac{1}{3} + b \cos^2\theta$ . The solid lines are the values obtained from the global fits for (a) 320–402 MeV and (b) 320–450 MeV. The dotted lines are extrapolations to higher energies.

of the  $\gamma$ -ray energy along with the angular distribution would have minimized these uncertainties. Cence *et al.* [23] did measure both energy and angular distribution of the  $\gamma$  at 735 MeV and were able to obtain a very precise measurement of the  $b$  parameter. The present results have very small uncertainties because we significantly improved the technique by measuring both the angular and energy distributions of the  $\pi^0$  mesons. The improvement is very clearly seen in Fig. 11. Unfortunately, the maximum energy available at TRIUMF is 500 MeV so we were unable to determine the  $b$  parameter from 500 to 750 MeV to map out the change in the character of the angular distribution. We have not included the preliminary results of Andreev *et al.* [54] from  $T_p = 600$  to 860 MeV which confirms that  $b$  rises to about 0.3, because, unfortunately, their results appear to have quite large energy to energy fluctuations. Although it is not clear how far we can extrapolate the results from our global fits due to the limited validity of the Gell-Mann–Watson functions, the extrapolated values of  $b$  (dotted lines in Fig. 11) are consistent with the experimental results of Dunaitsev and Prokoshkin and of Guzhavin *et al.*

### C. Comparison with $np \rightarrow NN\pi^\pm$

As mentioned in the Introduction there has been an ongoing interest concerning the value of  $\sigma_{01}$ . The normal practice in determining  $\sigma_{01}$  has been to use the total cross sections of the reactions  $pp \rightarrow pp\pi^0$  and  $np \rightarrow NN\pi^\pm$ . From entries (c), (f), and (g) of Table I

$$\sigma_{01} = 2\sigma(np \rightarrow NN\pi^\pm) - \sigma(pp \rightarrow pp\pi^0). \quad (17)$$

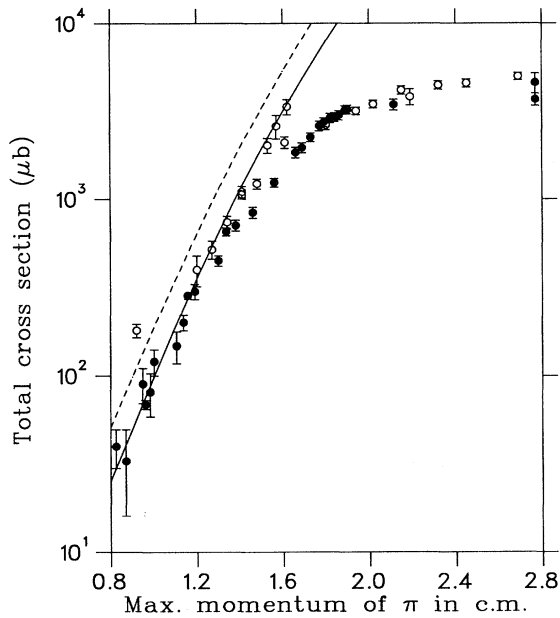


FIG. 12. Comparison of total cross sections for  $pp \rightarrow pp\pi^0$  (solid circles) and  $np \rightarrow \pi NN$  (open circles) plotted against the maximum pion momentum  $\eta$  which removes mass effects. The solid line is a global fit to our  $pp \rightarrow pp\pi^0$  data ( $\eta = 0.5-1.33$ ). The dashed line is our global fit plus some  $Sp$  and  $Pp$  terms of  $\sigma_{01}$  (see Table V). Handler's measurement [8] is at  $\eta = 0.92$ .

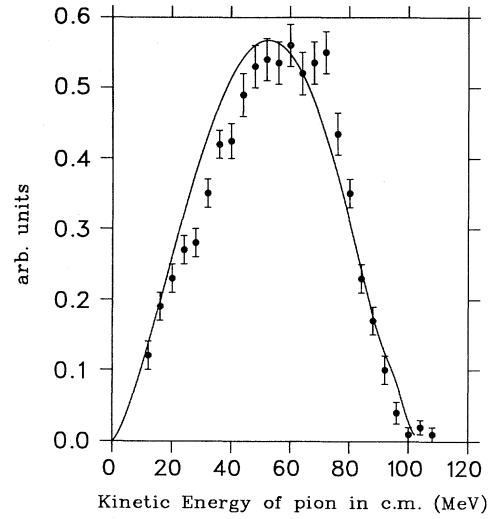


FIG. 13. Comparison of our data from  $pp \rightarrow pp\pi^0$  at 500 MeV (solid line) with the  $\pi^+$  data of Kleinschmidt *et al.* [9] for  $np \rightarrow \pi^+nn$  at the same energy. The  $\pi^0$  spectrum is corrected for the efficiency of the detector. The agreement indicates that the contribution from  $\sigma_{01}$  to the  $np$  data is either small or the same shape as the  $\sigma_{11}$  spectrum.

In Fig. 12 all the available data on  $\sigma(pp \rightarrow pp\pi^0)$  and  $2\sigma(np \rightarrow NN\pi^\pm)$  are presented. We have plotted the data according to the maximum momentum of the pion in the center of mass  $\eta_m$ , in units of  $\mu c$ , i.e., 140 MeV/c. This compensates to first order for the different phase space caused by the very different thresholds. Due to the obvi-

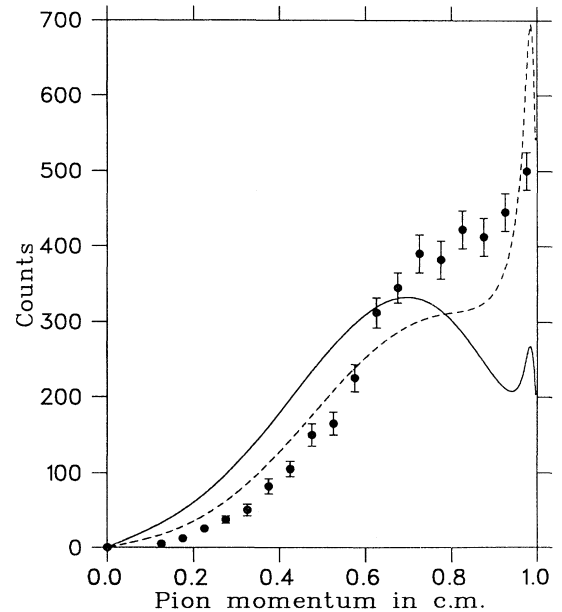


FIG. 14. Comparison of our  $\pi^0$  data from  $pp \rightarrow pp\pi^0$  at 402 MeV (solid line) with the  $\pi^-$  data of Handler for  $np \rightarrow \pi^-pp$ . The  $\pi^0$  spectrum is corrected for the efficiency of the detector. The  $pp \rightarrow pp\pi^0$  spectrum with an  $Sp$  and a  $Pp$  term of  $\sigma_{01}$  (see Table V) added to it is shown as a dashed line.

TABLE V. Suggested values for the transitions at 400 MeV for the reaction  $np \rightarrow \pi NN$  (in  $\mu\text{b}$ ).

$\frac{1}{2}\sigma_{01}$	$\frac{1}{2}\sigma_{11}$
$S_p=20$	$S_s=7$
	$P_s=6$
$P_p=10$	$P_p=21$

ous inconsistencies between the  $np$  total cross-section data in Fig. 12, it is extremely difficult to make any concrete conclusion from this plot, except that  $\sigma_{01}$  appears to be small. An obvious way to determine  $\sigma_{01}$  would be to fit both sets of data and do the subtraction. Such an approach was taken recently by Bystricky *et al.* [6] who used all the available inelastic nucleon-nucleon data and did a consistent fit. They found that above 3 GeV the  $I=1$  and  $I=0$  inelastic cross sections are of the same magnitude while below 600 MeV  $\sigma_{01}$  is small. They have

estimated the  $I=0$  cross sections in two different ways and obtained different results probably due to inconsistencies in the data. One obvious problem is the  $np$  datum at  $\eta_m \sim 1$ . This is Handler's measurement [8] and it seems to be too high.

Since there are indications that  $\sigma_{01}$  is relatively small in our energy region, one might expect the two reactions  $pp \rightarrow pp\pi^0$  and  $np \rightarrow NN\pi^\pm$  to be similar. One way of comparing the two reactions is to look at the angular distribution parameter  $b$ . We obtained  $b \sim 0.04$ , but, Kleinschmidt *et al.* [9] obtained  $b \sim 0.6$  for the  $np$  reaction. However, in this analysis they arbitrarily assumed that there was no  $\cos\theta$  term. A reanalysis by the same group later indicates that they need to include a  $\cos\theta$  term in their fit, but the  $\cos^2\theta$  term is likely to remain substantially larger than the same term for  $pp \rightarrow pp\pi^0$ . We await the results of their new analysis to compare in detail with  $pp\pi^0$ , but their measurements are similar to earlier results of Nikitin's group at Dubna [11], as well as Handler, so

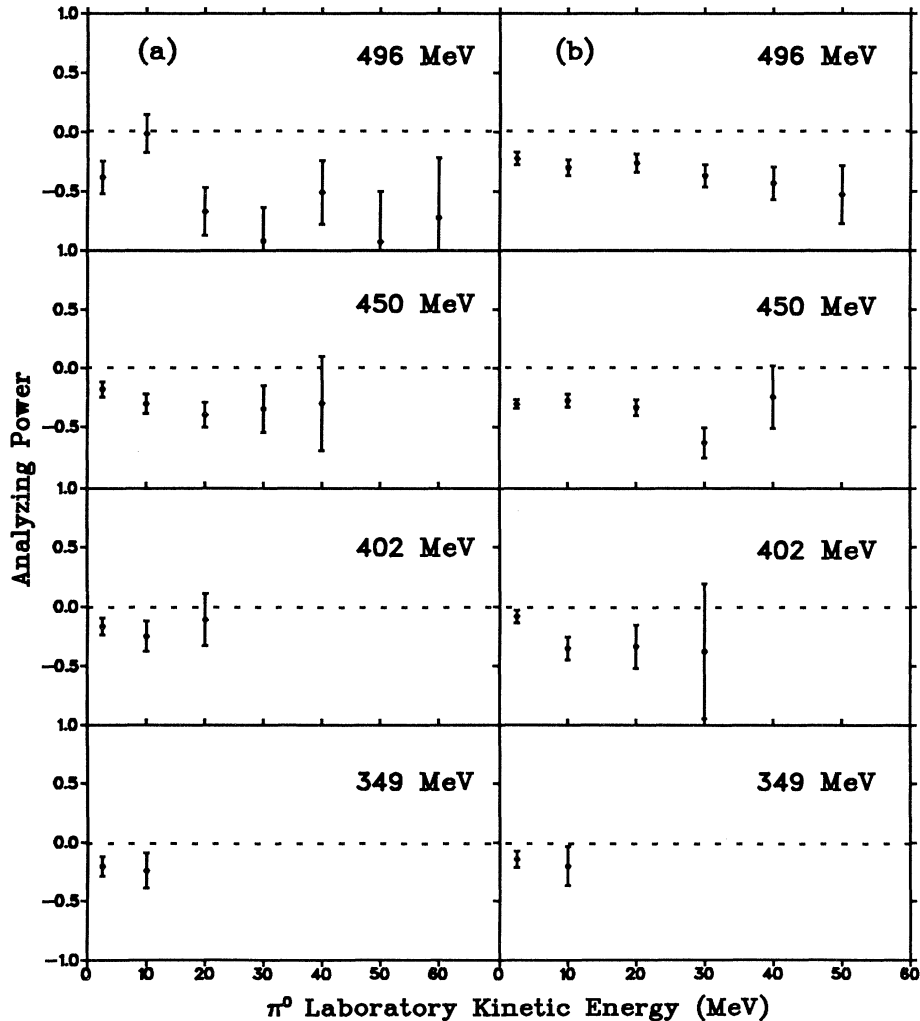


FIG. 15. Analyzing powers at the laboratory angle of (a)  $80^\circ$  and (b)  $90^\circ$  for incident proton energies of 496, 450, 402, and 350 MeV.

TABLE VI.  $\pi^0$  analyzing powers for the reaction  $p + p \rightarrow p + p + \pi^0$  obtained from the  $180^\circ$  geometry at 496 MeV.

$\pi^0$ laboratory angle (deg)	$\pi^0$ laboratory kinetic energy (MeV)	Analyzing power
40	2.5	0.18±0.16
	10	-0.37±0.31
	20	-0.54±0.33
	30	-0.53±0.33
	40	-0.21±0.33
	50	-0.53±0.27
	60	-0.27±0.34
	70	-0.64±0.30
	80	-0.62±0.29
	90	-0.36±0.31
60	100	-0.58±0.44
	110	-0.37±0.32
	2.5	-0.52±0.15
	10	-0.14±0.18
	20	-0.33±0.19
	30	-0.37±0.23
	40	-0.17±0.23
	50	-0.76±0.26
	60	-0.61±0.26

there is little doubt that significant  $\cos\theta$  and  $\cos^2\theta$  terms are needed to describe the  $\pi^\pm$  angular distribution. Thus there must be an contribution in these reactions from pion production in the  $I=0$  channel. (Note that at 800 MeV the  $\cos\theta$  term is insignificant [12].)

Yet another away of comparing the two reactions is to

TABLE VII.  $\pi^0$  analyzing powers for the reaction  $p + p \rightarrow p + p + \pi^0$  obtained from the  $180^\circ$  geometry at 496 MeV.

$\pi^0$ laboratory angle (deg)	$\pi^0$ laboratory kinetic energy (MeV)	Analyzing power
80	2.5	-0.38±0.14
	10	-0.01±0.16
	20	-0.67±0.20
	30	-0.93±0.29
	40	-0.51±0.27
	50	-0.93±0.43
	60	-0.72±0.50
90	2.5	-0.22±0.05
	10	-0.30±0.07
	20	-0.26±0.08
	30	-0.37±0.09
	40	-0.43±0.14
	50	-0.53±0.24
	100	-0.02±0.11
100	10	-0.26±0.13
	20	-0.40±0.15
	30	-0.68±0.24
	120	0.11±0.11
120	10	-0.35±0.16
	20	-0.70±0.47
	140	-0.09±0.09
140	10	-0.44±0.17
	20	-0.15±0.66

TABLE VIII.  $\pi^0$  analyzing powers for the reaction  $p + p \rightarrow p + p + \pi^0$  obtained from the  $180^\circ$  geometry at 450 MeV.

$\pi^0$ laboratory angle (deg)	$\pi^0$ laboratory kinetic energy (MeV)	Analyzing power	
40	2.5	-0.10±0.08	
	10	-0.10±0.15	
	20	0.01±0.17	
	30	-0.60±0.15	
	40	-0.01±0.15	
	50	-0.28±0.14	
	60	-0.15±0.16	
	70	-0.25±0.16	
	80	-0.25±0.26	
	90	-0.39±0.25	
60	100	-0.56±0.50	
	2.5	-0.33±0.09	
	10	-0.39±0.11	
	20	-0.39±0.11	
	30	-0.39±0.15	
	40	-0.18±0.13	
	50	-0.52±0.22	
	60	-0.56±0.34	
	80	2.5	-0.18±0.06
		10	-0.30±0.08
20		-0.40±0.11	
30		-0.35±0.20	
40		-0.30±0.40	

look at the energy spectra of the pion. In Fig. 13 the center-of-mass  $\pi^+$  energy spectrum of Kleinschmidt *et al.* [9] at 500 MeV as read off their figure is plotted along with the center-of-mass energy spectrum of  $\pi^0$  mesons obtained from the fit to our data. Since the maximum kinetic energy of the pions is different for the two reactions, mainly due to the small mass differences between  $\pi^0$  and  $\pi^+$ , and between the neutron and proton, our spectrum was scaled and normalized to their spectrum in order to be able to compare the shapes of the two

TABLE IX.  $\pi^0$  analyzing powers for the reaction  $p + p \rightarrow p + p + \pi^0$  obtained from the  $180^\circ$  geometry at 450 MeV.

$\pi^0$ laboratory angle (deg)	$\pi^0$ laboratory kinetic energy (MeV)	Analyzing power
90	2.5	-0.31±0.04
	10	-0.28±0.06
	20	-0.34±0.07
	30	-0.64±0.13
100	40	-0.25±0.27
	2.5	-0.13±0.06
	10	-0.21±0.09
	20	-0.43±0.13
120	30	-0.20±0.28
	2.5	-0.35±0.07
	10	-0.16±0.14
140	20	0.27±1.47
	2.5	-0.27±0.08
	10	-0.27±0.13

TABLE X.  $\pi^0$  analyzing powers for the reaction  $p + p \rightarrow p + p + \pi^0$  obtained from the  $180^\circ$  geometry at 402 MeV.

$\pi^0$ laboratory angle (deg)	$\pi^0$ laboratory kinetic energy (MeV)	Analyzing power
40	2.5	$-0.11 \pm 0.13$
	10	$-0.24 \pm 0.14$
	20	$-0.41 \pm 0.15$
	30	$-0.40 \pm 0.16$
	40	$-0.52 \pm 0.18$
	50	$-0.17 \pm 0.21$
	60	$0.45 \pm 0.54$
60	70	$0.25 \pm 1.13$
	2.5	$-0.14 \pm 0.07$
	10	$-0.30 \pm 0.08$
	20	$-0.32 \pm 0.10$
	30	$-0.22 \pm 0.13$
	40	$-0.36 \pm 0.15$
	50	$-0.49 \pm 0.40$
80	2.5	$-0.17 \pm 0.07$
	10	$-0.25 \pm 0.13$
	20	$-0.11 \pm 0.22$
90	2.5	$-0.08 \pm 0.05$
	10	$-0.35 \pm 0.10$
	20	$-0.33 \pm 0.18$
	30	$-0.38 \pm 0.57$
100	2.5	$-0.17 \pm 0.07$
	10	$-0.35 \pm 0.12$
120	2.5	$-0.15 \pm 0.08$
	10	$-0.12 \pm 0.56$
140	2.5	$-0.13 \pm 0.17$

spectra. Now, if there is a difference between the two reactions (due to  $\sigma_{01}$ ), the two spectra could be different, but clearly they are very similar apart from the very small bump seen in the  $pp \rightarrow pp\pi^0$  spectrum at the highest energy due to the  $Ss$  transition. Similarly Thomas *et al.* [12] found that the  $\pi^+$  and  $\pi^-$  spectra from  $np$  collisions were almost identical at 800 MeV. As no significant difference is seen in such comparisons,  $\sigma_{01}$  is probably small relative to  $\sigma_{11}$ , although an alternate explanation is

that  $\sigma_{01}$  and  $\sigma_{11}$  are the same shape. This is unlikely as we shall see from the evidence at 400 MeV.

Around 400 MeV a very different situation seems to occur. We have compared the center-of-mass  $\pi^-$  momentum spectrum of Handler [8] from the reaction  $np \rightarrow pp\pi^-$  with that obtained from our global fit [50,53] (Fig. 14). The solid line is our global fit normalized to the spectrum and is clearly very different. Most of the difference can be attributed to the fact that the  $np \rightarrow pp\pi^-$  reaction has an  $S_p$  transition (from  $\sigma_{01}$ ) which is not available to the  $Pp \rightarrow pp\pi^0$  reaction. This term enhances the peak at the highest pion momentum and also produces the  $\cos\theta$  term observed in the angular distribution. In addition, we should note that the spectrum obtained by Handler was for an incident neutron energy spectrum ranging from threshold to 440 MeV. The spectrum plotted from our results is for 409 MeV, the mean energy of his neutron spectrum. It is not clear how to weight the contributions from different energies. There are other factors to consider too. Handler found that the contribution from the  $P_s$  transition was negligible ( $\sim 1\%$ ). In our analysis a fairly significant  $P_s$  term was observed [50,53], though it decreases in favor of the  $P_p$  transitions as the energy increases. We observe fairly large asymmetries and their shape are also in favor of a non-negligible  $P_s$  term. For the  $P_p$  transition Handler suggested that the contribution from  $\sigma_{11}$  was larger than that from  $\sigma_{01}$ . Overall his conclusion was that  $\sigma_{01}$  was comparable to  $\sigma_{11}$ , if not larger. The fairly significant differences seen between the two spectra of Fig. 14 also suggest a large  $\sigma_{01}$  (as compared to  $\sigma_{11}$ ). Now if we use Handler's value of  $\sigma_{np} = 90 \mu\text{b}$  and our fit value for  $\sigma_{11}$  at  $\eta = 0.92$  ( $58 \mu\text{b}$ ), we can estimate  $\sigma_{01} = 2\sigma_{np} - \sigma_{11} = 122 \mu\text{b}$ . This is very large and would yield inconsistencies with other total cross-section measurements of  $np \rightarrow \pi NN$  at higher energies. Other estimates for this cross section can be obtained from pion absorption in  $^3\text{He}$  (Refs. [55] and [56]). These measurements find that the  $\sigma_{01}$   $S_p$  term is  $19 \pm 4 \mu\text{b}$  at 409 MeV and  $31 \pm 6 \mu\text{b}$  at 442 MeV. A recent measurement by Ponting *et al.* [57] has been made of the pion asymmetry in the reaction  $np \rightarrow \pi^- pp$  at 400 MeV for the pions on the high-energy peak. They find

TABLE XI.  $\pi^0$  analyzing powers for the reaction  $p + p \rightarrow p + p + \pi^0$  obtained from the  $180^\circ$  geometry at 349 and 319 MeV.

Proton energy (MeV)	$\pi^0$ laboratory angle (deg)	$\pi^0$ laboratory kinetic energy (MeV)	Analyzing power
349	60	2.5	$0.19 \pm 0.27$
		10	$-0.16 \pm 0.35$
		20	$-0.06 \pm 0.49$
	80	2.5	$-0.20 \pm 0.08$
		10	$-0.24 \pm 0.15$
		2.5	$-0.14 \pm 0.07$
	90	10	$-0.20 \pm 0.17$
		2.5	$-0.12 \pm 0.12$
		10	$-0.63 \pm 0.81$
	100	2.5	$-0.49 \pm 0.86$
		10	$-0.50 \pm 0.90$
		2.5	$-0.04 \pm 0.08$
320	90	2.5	$-0.04 \pm 0.08$

TABLE XII.  $\pi^0$  analyzing powers for the reaction  $p + p \rightarrow p + p + \pi^0$  obtained from the symmetric geometry at 496 MeV.

Geometry	$\pi^0$ laboratory angle (deg)	$\pi^0$ laboratory kinetic energy (MeV)	Analyzing power
60°-60°	1	20	-0.14±0.16
	30	30	-0.38±0.14
	38	40	-0.55±0.14
	43	50	-0.75±0.14
	46	60	-0.41±0.13
	48	70	-0.49±0.16
	50	80	-0.30±0.16
	51	90	-0.68±0.25
	52	100	-0.47±0.38
	70°-70°	0	2.5
20		10	0.17±0.17
46		20	-0.48±0.16
53		30	-0.23±0.16
57		40	-0.52±0.15
60		50	-0.19±0.16
62		60	-0.60±0.17
80°-80°	4	2.5	-0.21±0.09
	61	10	-0.36±0.12
	69	20	-0.35±0.13
	72	30	-0.53±0.15
	74	40	-0.47±0.15
	75	50	-0.57±0.22
	76	60	-0.44±0.43

TABLE XIII.  $\pi^0$  analyzing powers for the reaction  $p + p \rightarrow p + p + \pi^0$  obtained from the symmetric geometry at 450 and 402 MeV.

Proton energy (MeV)	Geometry	$\pi^0$ laboratory angle (deg)	$\pi^0$ laboratory kinetic energy (MeV)	Analyzing power
450	40°-40°	0	70	-0.22±0.09
		10	80	-0.27±0.08
		17	90	-0.47±0.08
		21	100	-0.28±0.09
		23	110	-0.42±0.13
		25	120	-0.20±0.17
		27	130	-0.11±0.26
		28	140	-0.29±0.45
	60°-60°	1	20	-0.31±0.10
		30	30	-0.47±0.10
		38	40	-0.47±0.10
		43	50	-0.64±0.11
		46	60	-0.39±0.14
		48	70	-0.77±0.15
402	40°-40°	50	80	-0.26±0.34
		0	70	-0.19±0.10
		10	80	-0.25±0.11
		17	90	-0.18±0.26
		1	20	-0.49±0.07
	60°-60°	30	30	-0.22±0.08
		38	40	-0.40±0.09
		43	50	-0.37±0.13
		46	60	-0.41±0.27

that the  $Sp$  term is made up equally of the transitions  ${}^3S_1 \rightarrow {}^1S_0 p_1$  and  ${}^3D_1 \rightarrow {}^1S_0 p_1$ . They also require very little  $\sigma_{11}$  contribution from  ${}^3P_0 \rightarrow {}^1S_0 s_0$  which is compatible with our observation. To initiate discussion we suggest a possible solution to the 400 MeV case in Table V. We use our values for  $\sigma_{11}$  and informed guesses for the  $\sigma_{01}$  intensities. Thus to compare our results with Handler we use these values in Table V; i.e., we have to add to our fit an  $Sp$  term, which is three times the  $Ss$  term, and also add a small  $Pp$  term. If we use the resolution of Handler's experiment of  $\sigma=0.011$  and allow the normalization to float we obtain the dashed curve in Fig. 14 which is certainly better, though far from perfect.

To see how this would be compatible with higher-energy  $np$  work we took our global fit (solid line in Fig. 12) and added this amount of  $Sp$  and  $Pp$  with the normal energy dependence and obtained the dashed line in Fig. 12. Handler's point at  $\eta=0.92$  is clearly too high because the dashed line goes above all other  $np$  data, and so we suggest he had a normalization error. There are also clear inconsistencies between the  $np$  data at  $\eta=1.6$  and those at  $\eta > 1.9$ .

#### D. Analyzing power

The  $\pi^0$  analyzing powers obtained in this investigation are listed in Tables VI–XIII and some are illustrated in Fig. 15. These are the first such measurements for the reaction  $pp \rightarrow pp\pi^0$ . The large asymmetry observed is principally a result of the interference between the  $Ps$  and  $Pp$  transitions, as all other terms are relatively small and is consistent with the fairly similar cross sections for the  $Ps$  and  $Pp$  transitions [50,53]. The sign of the asymmetry is negative, the same as observed in the  $pp \rightarrow \pi^+ d$  and  $pp \rightarrow pn\pi^+$  reactions [58]. In an experiment at Indiana, Korkmaz *et al.* [59] have found that there is evidence from the  ${}^{13}\text{C}(p, \pi^-)$  reaction at 200 MeV suggesting that the asymmetry for  $pn \rightarrow \pi^- pp$  might be positive. However, for the only free results available which are at 400 MeV and for the peak region only, a swing from positive to negative is found [57]. Similar results are found in recent unpublished data from the same group at nearby energies. According to their 400 MeV analysis, the peak region is almost exclusively  $T=0$ , which is not totally compatible with our results. Hence we need  $\pi^\pm$  asymmetries from free  $np$  collisions to settle this puzzle. Since Handler and also Ponting *et al.* have found  $\sigma_{01}$  to be important at 400 MeV, it would not be strange if the asymmetries for  $np \rightarrow NN\pi^\pm$  and  $pp \rightarrow pp\pi^0$  were quite

different in our energy range. Unfortunately at the present moment there are no theoretical predictions for this observable and hence no comparisons can be made.

#### V. SUMMARY AND CONCLUSIONS

We have measured the total and differential cross sections and the analyzing powers of the  $\pi^0$  energy spectra for the reaction  $pp \rightarrow pp\pi^0$  for five incident proton energies between 319 and 496 MeV. This was done by detecting the  $\gamma$  rays from the decay of the  $\pi^0$ . The cross sections were determined by fitting to the experimental data the center-of-mass  $\pi^0$  energy functions which were derived by Gell-Mann. Simultaneous fits were performed to all the  $\pi^0$  energy spectra of a given proton energy. Our results for the total cross sections are consistent with the earlier measurements but are of much higher precision. Similarly for the  $\pi^0$  angular distributions we observe a very small  $\cos^2\theta$  term.

The shape of the center-of-mass energy spectrum of the  $\pi^0$  mesons from the reaction  $pp \rightarrow pp\pi^0$  is very similar to that of the  $\pi^+$  mesons from the reaction  $np \rightarrow nn\pi^+$  at 500 MeV, but at 409 MeV the  $\pi^-$  energy spectrum from the reaction  $np \rightarrow pp\pi^-$  is quite different from that of the  $\pi^0$  mesons. The  $\sigma_{01}$  term is likely to be mainly an  $Sp$  transition which increases as  $\eta_0^4$  so that at 409 MeV it could be important, but at higher energies it could become relatively smaller because the  $Ps$  and  $Pp$  terms increase even faster with energy. The total cross sections also favor the supposition that  $\sigma_{01}/\sigma_{11}$  decreases at higher energies, but  $\sigma_{01}$  certainly does not go to zero as the  $\pi^\pm$  angular distributions from the SIN and Dubna data both indicate an important  $\cos\theta$  term as well as a  $\cos^2\theta$  term which is larger than that for  $\sigma_{11}$ .

Our results for the analyzing powers are the first measurements of this observable for the reaction  $pp \rightarrow pp\pi^0$ . The values are fairly independent of angle and energy and are all significantly negative, which is the opposite sign of the suggested asymmetry for  $np \rightarrow \pi^- pp$ .

Overall the results we have obtained are a considerable improvement over the existing  $\sigma_{11}$  data. The next task is clearly to tackle pion production in  $np$  collisions. The most sensitive reactions are  $np \rightarrow \pi^- pp$  and  $np \rightarrow \pi^+ nn$  and it will be necessary to measure several parameters, but most importantly it will be essential to investigate quite a few energies because of the rapid relative variation of the production amplitudes near threshold.

\*Present address: Los Alamos National Laboratory, MS H846, Los Alamos, NM 87545.

†On leave from Central Research Institute for Physics, H-1525 Budapest, Hungary.

- [1] K. M. Watson and K. A. Brueckner, Phys. Rev. **83**, 1 (1951).
- [2] A. H. Rosenfeld, Phys. Rev. **96**, 139 (1954).
- [3] D. V. Bugg, Annu. Rev. Nucl. Sci. **35**, 295 (1985).
- [4] D. V. Bugg, A. Hasan, and R. L. Shypit, Nucl. Phys.

A477, 546 (1988); F. Arash, M. J. Moravcsik, G. R. Goldstein, and D. V. Bugg, Phys. Rev. Lett. **62**, 517 (1989).

- [5] B. J. VerWest and R. A. Arndt, Phys. Rev. C **25**, 1979 (1982).
- [6] J. Bystricky, P. La France, F. Lehar, F. Perrot, T. Siemiarczuk, and P. Winternitz, J. Phys. **48**, 1901 (1987).
- [7] S. Mandelstam, Proc. Roy. Soc. London **A244**, 491 (1958).
- [8] R. Handler, Phys. Rev. **138**, 1230B (1965).
- [9] M. Kleinschmidt, T. Fisher, G. Hammel, W. Hurster, K.

- Kern, L. Lehmann, E. Rössle, and H. Schmitt, *Z. Phys. A* **298**, 253 (1980).
- [10] H. Fisher, J. Franz, V. Grundies, S. Jacoby, A. Klett, P. Koncz, M. Marx, E. Rössle, C. Sauerwein, H. Schleder-  
mann, H. Schmitt, and H. L. Woolverton, *Pion Production in Neutron-Proton Collisions*, SIN Newsletter 19 SIN (Vil-  
ligen, 1987).
- [11] A. Abdivaliev *et al.*, Dubna Report JINR D1-81-756, 1981.
- [12] W. Thomas, R. Carlini, C. Cassapakis, B. Dieterle, J. Donahue, C. Leavitt, T. Rupp, D. Wolfe, M. L. Evans, G. Glass, M. Jain, L. Northcliffe, B. Bonner, and J. Simmons, *Phys. Rev. D* **24**, 1736 (1981).
- [13] L. G. Dakhno, A. V. Kravtsov, E. A. Lobachev, M. M. Makarov, V. I. Medvedev, G. Z. Obrant, V. I. Poromov, V. V. Sarantsev, V. M. Sirin, G. L. Sokolov, and S. G. Sherman, *Phys. Lett.* **114B**, 409 (1982).
- [14] J. Marshall, L. Marshall, V. A. Nedzel, and S. D. Warshaw, *Phys. Rev.* **88**, 632 (1952).
- [15] J. W. Mather and E. A. Martinelli, *Phys. Rev.* **92**, 780 (1953).
- [16] L. M. Soroko, *Zh. Eksp. Teor. Fiz.* **30**, 296 (1956) [*Sov. Phys. JETP* **3**, 184 (1956)].
- [17] B. J. Moyer and R. K. Squire, *Phys. Rev.* **107**, 283 (1957).
- [18] Yu. D. Prokoshkin and A. A. Tiapkin, *Zh. Eksp. Teor. Fiz.* **32**, 750 (1957) [*Sov. Phys. JETP* **5**, 618 (1957)].
- [19] R. A. Stallwood, R. B. Sutton, T. H. Fields, J. G. Fox, and J. A. Kane, *Phys. Rev.* **109**, 1716 (1958).
- [20] A. F. Dunaitsev and Yu. D. Prokoshkin, *Zh. Eksp. Teor. Fiz.* **36**, 1656 (1959) [*Sov. Phys. JETP* **9**, 1179 (1959)].
- [21] F. Shimizu, Y. Kubota, H. Koiso, F. Sai, S. Sakamoto, and S. S. Yamamoto, *Nucl. Phys.* **A386**, 571 (1982).
- [22] H. O. Meyer, M. A. Ross, R. E. Pollock, A. Berdoz, F. Dohrmann, J. E. Goodwin, M. G. Minty, H. Nann, P. V. Pancella, S. F. Pate, B. V. Przewoski, T. Rinckel, and F. Sperisen, *Phys. Rev. Lett.* **65**, 2846 (1990); *Nucl. Phys.* (to be published).
- [23] R. J. Cence, D. L. Lind, G. D. Mead, and B. J. Moyer, *Phys. Rev.* **131**, 2713 (1963).
- [24] V. M. Guzhavin, G. K. Kliger, V. Z. Kolganov, A. V. Lebedev, K. S. Marish, Yu. D. Prokoshkin, V. T. Smolyan-  
kin, A. P. Sokolov, L. M. Soroko, and Ts'ui Wa-Ch'uang, *Zh. Eksp. Teor. Fiz.* **46**, 1245 (1964) [*Sov. Phys. JETP* **19**, 847 (1964)].
- [25] D. S. Beder, *Nuovo Cimento* **56A**, 625 (1968).
- [26] R. Baier and H. Kühnelt, *Nuovo Cimento* **63A**, 135 (1969).
- [27] M. Schillaci, R. R. Silbar, and J. E. Young, *Phys. Rev.* **179**, 1539 (1969).
- [28] D. Drechsel and H. J. Weber, *Nucl. Phys.* **B25**, 159 (1970).
- [29] E. Ferrari and F. Selleri, *Nuovo Cimento* **27**, 1450 (1963).
- [30] U. Amaldi, Jr., *Rev. Mod. Phys.* **39**, 649 (1967).
- [31] Y. Avishai and T. Mizutani, *Nucl. Phys.* **A326**, 352 (1979).
- [32] Y. Avishai and T. Mizutani, *Phys. Rev. C* **27**, 312 (1983).
- [33] H. Tanabe and K. Ohta, *Phys. Rev. C* **36**, 2495 (1987).
- [34] T. Ueda, *Nucl. Phys.* **A463**, 69 (1987).
- [35] T.-S. H. Lee and A. Matsuyama, *Phys. Rev. C* **36**, 1459 (1987).
- [36] F. Hachenberg and H. J. Pirner, *Ann. Phys. (N.Y.)* **112**, 401 (1978).
- [37] V. P. Efrosinin, D. A. Zaikin, and I. I. Osipchuk, *Z. Phys. A* **322**, 322 (1985).
- [38] A. König and P. Kroll, *Nucl. Phys.* **A356**, 345 (1981).
- [39] W. M. Kloet and R. R. Silbar, *Nucl. Phys.* **A338**, 281 (1980).
- [40] J. Dubach, W. M. Kloet, and R. R. Silbar, *Nucl. Phys.* **A466**, 573 (1987).
- [41] Z.-J. Cao and W.-Y. B. Hwang, *Phys. Rev. C* **34**, 1785 (1986).
- [42] M. Harvey, J. Letourneux, and B. Lorazo, *Nucl. Phys.* **A424**, 428 (1984).
- [43] K. Choi, K. Kang, and J. E. Kim, *Phys. Rev. Lett.* **62**, 849 (1989).
- [44] B. Bassalleck, F. Corriveau, M. D. Hasinoff, T. Marks, D. F. Measday, J.-M. Poutissou, and M. Salomon, *Nucl. Phys.* **A362**, 445 (1981).
- [45] M. Salomon, D. F. Measday, J.-M. Poutissou, and B. C. Robertson, *Nucl. Phys.* **A414**, 493 (1984).
- [46] R. L. Ford and W. R. Nelson, The EGS code system: com-  
puter programs for the Monte Carlo simulation of elec-  
tromagnetic cascade showers (version 3) (1978).
- [47] A. Bagheri, Ph.D. thesis, University of British Columbia, 1986.
- [48] M. Gell-Mann and K. M. Watson, *Annu. Rev. Nucl. Sci.* **4**, 219 (1954).
- [49] F. James and M. Roos, *Comput. Phys. Commun.* **10**, 343 (1975).
- [50] S. Stanislaus, Ph.D. thesis, University of British Columbia, 1988.
- [51] H. H. Barschall and W. Haeberli, The University of  
Wisconsin report, 1970.
- [52] T. Reposeur, J.-P. Didelez, M. A. Duval, R. Frascaria, R. Siebert, E. Warde, G. S. Blanpied, B. M. Preedom, B. Sanghai, G. Battistoni, C. Bloise, L. Satta, E. Bovet, J.-P. Egger, and F. Hinterberger, *Nucl. Phys.* **A508**, 650c (1990).
- [53] S. Stanislaus, D. Horvath, D. F. Measday, A. J. Noble, and M. Salomon, *Phys. Rev. C* **41**, R1913 (1990).
- [54] V. P. Andreev, A. V. Krastov, M. M. Makarov, V. I. Medvedev, V. I. Poromov, V. V. Sarantsev, S. G. Sher-  
man, G. L. Sokolov, A. B. Sokornov, and V. A. Trofimov, *Proceedings of the Third International Symposium on the Pion-Nucleon and Nucleon-Nucleon Physics*, Leningrad, (Academy of Sciences of the USSR, Leningrad, 1989), Vol. 2, p. 148.
- [55] K. A. Aniol, A. Altman, R. R. Johnson, H. W. Roser, R. Tacik, U. Wienands, D. Ashery, J. Alster, M. A. Moines-  
ter, E. Piasetzky, D. R. Gill, and J. Vincent, *Phys. Rev. C* **33**, 1714 (1986); M. A. Moinester, D. R. Gill, J. Vincent, D. Ashery, S. Levenson, J. Alster, A. Altman, J. Lichten-  
stadt, E. Piasetzky, K. A. Aniol, R. R. Johnson, H. W. Roser, T. Tacik, W. Gyles, and B. Barnett, *Phys. Rev. Lett.* **52**, 1203 (1984).
- [56] E. Piasetzky, D. Ashery, M. A. Moinester, G. A. Miller, and A. Gal, *Phys. Rev. Lett.* **57**, 2135 (1986).
- [57] C. Ponting, D. A. Hutcheon, M. A. Moinester, P. L. Wal-  
den, D. R. Gill, R. R. Johnson, F. Duncan, G. Sheffer, P. Weber, V. Sossi, A. Feltham, M. Hanna, R. Olszewski, M. Pavan, F. M. Rozon, M. Seviar, D. Ashery, R. P. Trelle, H. Hahn, and B. Mayer, *Phys. Rev. Lett.* **63**, 1792 (1989).
- [58] W. R. Falk, E. G. Auld, G. Giles, G. Jones, G. J. Lolos, W. Ziegler, and P. L. Walden, *Phys. Rev. C* **32**, 1972 (1985).
- [59] E. Korkmaz, L. C. Bland, W. W. Jacobs, T. G. Throwe, S. E. Vidgor, M. C. Green, P. L. Jolivet, and J. D. Brown, *Phys. Rev. Lett.* **58**, 104 (1987).